Electronic Supplemental Information (ESI)

2D stress-distribution imaging using 3D transparent stimulus-responsive color-changing rubber

Hazuki Yamanaka,[a] Hiroaki Imai,[a] Syuji Fujii,*[,b,c] Yuya Oaki*[,a]

[a] Department of Applied Chemistry, Faculty of Science and Technology, Keio University, 3-14-1 Hiyoshi, Kohoku-ku, Yokohama 223-8522, Japan.

[b] Department of Applied Chemistry, Faculty of Engineering, Osaka Institute of Technology, 5-16-1 Omiya, Asahi-ku, Osaka 535-8585, Japan.

[c] Department of Chemistry, Faculty of Science, Chulalongkorn University, Bangkok 10330, Thailand.

*E-mail: syuji.fujii@oit.ac.jp, oakiyuya@applc.keio.ac.jp

Contents

Detection range of compression stresses in previous works

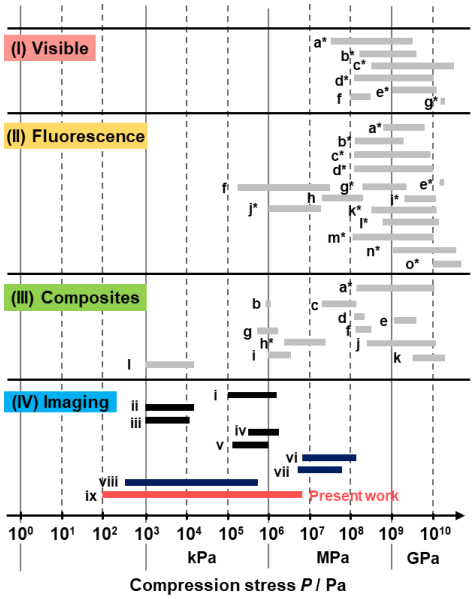

Fig. S1. Summary of previous works about compression-stress sensing. (I) Visible-light detection without UV-light excitation and matrix polymer. (II) Fluorescent detection without matrix polymer. (III) Composite type with the other matrix polymers and materials. (IV) Distribution imaging. The isotropic compression, such as hydrostatic pressing and diamond anvil cell, was noted with asterisk. The reference numbers correspond to those in the following lists for the groups (I)–(III) and in the main text for the group (IV).[19–26]

The similar comparison chart in our previous work was updated with addition of new works and modification of the classification.[25]

Additional References

(i) Visible: (a) Y. Liu, Q. Zeng, B. Zou, Y. Liu, B. Xu and W. Tian, *Angew. Chem. Int. Ed.*, 2018, **57**, 15670. (b) Q. Luo, C. Lv, H. Sheng, F. Cao, J. Sun, C. Zhang, M. Ouyang, B. Zou and Y. Zhang, *Adv. Opt. Mater.*, 2020, **8**, 1901836. (c) M. Liu, Z. Fu, R. Sun, J. Yuan, C. Liu, B. Zou, B. Wang, H. Kou, *ACS Appl. Electron. Mater.*, 2021, **3**, 1368. (d) X Wang, C. Qi, Z. Fu, H. Zhang, J. Wang, H. Feng, K. Wang, B. Zou, J. w. Y. Lam and B. Z. Tang, *Mater. Horiz.*, 2021, **8**, 630. (e) Y. Wang, X. Tan, Y. Zhang, S. Zhu, I. Zhang, B. Yu, K. Wang, B. Yang, M. Li, B. Zou and S. Zhang, *J. Am. Chem. Soc*., 2015, **137**, 931. (f) K. Ogumi, Y. Matsuo, K. Nagata, Y. Takimoto, K. Mishiba and Y. Matsuo, *J. Mater. Chem. C*, 2022, **10**, 11181. (g) T. Nishiuchi, S. Aibara, T. Yamakado, R. Kimura, S. Saito, H. Sato and T. Kubo, *Chem. Eur. J.*, 2022, **28**, e202200286.

(ii) Fluorescence: (a) Y. Dong, B. Xu, J. Zhang, X. Tan, L. Wang, J. Chan, H. Lv, S. Wen, B. Li, L. Ye, B. Zou and W. Tian, *Angew. Chem. Int. Ed.*, 2012, **51**, 10782. (b) K. Nagura, S. Saito, H.

Yusa, H. Yamawaki, H. Fujihisa, H. Sato, Y. Shimoikeda and S. Yamaguchi, *J. Am. Chem. Soc.*, 2013, **135**, 10322. (c) H. Yuan, K. Wang, K. Yang, B. Liu and B. Zou, *J. Phys. Chem. Lett.*, 2014, **5**, 2968. (d) Z. Gao, K. Wang, F. Liu, C. Feng, X. He, J. Li, B. Yang, B. Zou and P. Lu, *Chem. Eur. J.*, 2017, *23*, 773. (e) S. Lu, G. Xiao, L. Sui, T. Feng, X. Yong, S. Zhu, B. Li, Z. Liu, B. Zou, M. Jin, J. S. Tse, H. Yan and B. Yang, *Angew. Chem. Int. Ed*., 2017, **56**, 6187. (f) W Yin, Z. Yang, S. Zhang, Y. Yang, L. Zhao, Z. Li, B. Zhang, S. Zhang, B. Han and H. Ma, *J. Mater. Chem. C*., 2021, **5**, 2849. (g) M. Andrzejewski, N. Casati and A. Katrusiak, *Dalton Trans*. 2017, **46**, 14795. (h) B Poggi, L. Bodelot, M. Louis, R. Metivier and C. Allain, *J. Mater. Chem. C.*, 2021, **9**, 12111. (i) Z. Ding, T. Lu, C. Bi, B. Li, S. T. Zhang, W. Xu and S. Jiang, *Mater. Chem. Front.*, 2021*,* **6**, 86. (j) S. Wang, W. Xiang, C. Pan, J. Chen, W. Li, J. Zhang, J. Zhao and G. Liu, *CrystEngComm*, 2023, **25**, 3861. (k) A. Li, H. Liu, C. Song, Y. Geng, S. Xu, H. Zhang, H. Zhang, H. Cuib and W. Xu, *Mater. Chem. Front.*, 2019, **3**, 2128. (l) L. Ye, C. Lv, Y. Yao, K. Wang, Q. Song, K. Wang, C. Zhang and Y. Zhang, *ChemistrySelect*, 2022, **7**, e202201148. (m) Y. Gu, X. Sun, M. Wuc and K. Wang, *Phys. Chem. Chem. Phys.*, 2023, **25**, 17264. (n) L. Gao, C. Bi, F. Liu, Z. Feng, C. Sun, S. Xu, W. Xu and P. Lu, *Adv. Opt. Mater.*, 2022, **10**, 2102321. (o) J. Yang, Z. Fu, H. Ma, T. Wang, Q. Li, K. Wang, L. Wu, P. Chen, H. Feng and B. Tang, *ACS Mater. Lett.*, 2023, **5**, 1441.

(iii) Composites: (a) H. Yang, Z. Sun, C. Lv, M. Qile, K. Wang, H. Cao, B. Zou, Q. Song and Y. Zhang, *ChemPlusChem*, 2018, **83**, 132. (b) Z. Liu, H. Bisoyi, Y. Huang, M. Wang, H. Yang and Q. Li, *Angew. Chem. Int. Ed.*, 2022, **61**, e202115755. (c) D. A. Davis, A. Hamilton, J. Yang, L. D. Cremar, D. V. Gough, S. L. Potisek, M. T. Ong, P. V. Braun, T. J. Martinez, S. R. White, J. S. Moore and N. R. Sottos, *Nature*, 2009, **459**, 68. (d) C. E. Diesendruck, B. D. Steinberg, N. Sugai, M. N. Silberstein, N. R. Sottos, S. R. White, P. V. Braun and J. S. Moore, *J. Am. Chem. Soc.*, 2012, **154**, 12446. (e) R. Toivola, P. Lai, J. Yang, S. Jang, A. K. Y. Jen and B. D. Flinn, *Comp Sci. Tech*., 2017, **139**, 74. (f) Z. Wang, Z. Ma, Y. Wang, Z. Xu, Y. Luo, Y. Wie and X. Jia, *Adv. Mater.*, 2015, **27**, 6469.(g) D. Han, X. Wang, S. Liu, Y. Zhang, C. Li, Y. Gao and J. Zhang, *Adv. Mater. Technol.*, 2023, **8**, 2300175. (h) Y. Sagara, N. Tamaoki and G. Fukuhara, *ChemPhotoChem*, 2018, **2**, 959. (i) B. Xu, Z. Luo, R. Xiao, Z. Wang and J. Yang, *Macromol. Rapid Commun.*, 2022, **43**, 2200580. (j) Z. Chen, F. Ye, T. Shao, Y. Wu, M. Chen, Y. Zhang, X. Zhao, B. Zou and Y. Ma, *Macromolecules*, 2022, **55**, 2310. (k) Y. Lai, M. Chen, Y. Wu, Y. Zhang, X. Zhao and Z. Chen, *J Appl Polym Sci*., 2022, **139**, e52898. (l) Z. Wang, J. Zhang, Z. Lan, Q. Meng, R. Tang, X. Shen and Q. Sun, *Adv. Mater. Interfaces*, 2022, **9**, 2102047.

(iv) Imaging: (a) 19. (b) 20. (c) 21. (d) 22. (e) 23. (f) 24. (g) 37. (h) 39. The reference numbers correspond to those in the main text.

Experimental methods

Preparation of DL/SR/PDA device. SR/PDA was prepared by the method referred to the previous report.[41] Chloroform (Kanto 99 %) solution (2 cm^3) containing 2.5 mg of PCDA (TCI 97 %) was prepared and then filtered to remove the red precipitate as the already polymerized material. The chloroform solution (1.5 cm^3) was added to 5 g of a silicone precursor (Shinetsu KE-108) in a polypropylene vessel (60 mm in diameter and 31 mm in height) at room temperature. This silicone source is comprised of the main and curing agents with the condensation polymerization. The mixture solution was set under vacuum condition at room temperature to remove chloroform. The PCDA precipitates dispersed in the silicone precursor were polymerized with the UV-light irradiation (a handy lamp, 254 nm, 6 W) for ca. 1 min under manual mixing. A curing agent (0.5 g) was added to the silicone solution with the dispersion of PDA and then maintained at room temperature for 72 h. SR/PDA was cut a piece 10 × 10 × 3 mm in size to obtain the relationship between P and Δx for the standard curve and 30 × 30 × 3 mm in size for the stress-distribution imaging.

The interior liquid for DL was prepared by mixing 12.5 g PEI (Nippon Shokubai, EPOMIN SP-003, 98 %, branched PEI with $\bar{M}_w$ 3×10^2) and 12.5 g purified water. The standard PEI concentration was 50 wt% in the present study. DL was prepared by mixing 2.778 g silica (SiO_2) particles modified with polydimethylsiloxane (PDMS) (Aerosil RY-300, 21–27 nm) and 25 g of the interior liquid using a mixer (LabMill, Osaka Chemical) at 20000 rpm for 5 s. The resultant DL was separated using stainless sieves with the pore sizes 125 and 250 μm. The sieved DL was stored in a polypropylene bottle with sealing until the use. Before the compression experiment, ca. 50 and 450 mg of DL was dispersed on the top face of a piece of SR/PDA 10 × 10 × 3 mm and 30 × 30 × 3 mm in size, respectively.

Structural characterization. Macroscopic images of the samples were taken using iPhone 14. The microscopic morphologies were observed by optical microscopy (Keyence, VHX1100) and scanning electron microscopy (Zeiss, Merlin compact VP). The particle size of DL was measured on the optical microscopy images. The layered structure was analyzed by X-ray diffraction (Bruker, D8 Advance). The polymerization behavior of PCDA was studied using Raman spectroscopy with the excitation at 785 nm (Renishaw, In-via Raman). The transparency and absorbance of the SR/PDA samples were measured using a UV-Vis spectrophotometer (Jasco, V-670). Free-volume space of SR and SR/PDA was measured using positron

annihilation lifetime spectroscopy (Toyo Seiko).

Analysis of color-change properties. Prior to the compression experiment, the thermoresponsive color-change properties were analyzed. SR/PDA and its reference PDA powder were heated on a temperature-controlled stage in the range of 20−100 °C. Afte The photograph of the sample was taken 1 min after reaching at a certain temperature. The RGB values were estimated from the photographs using ImageJ software and then converted to *XYZ* ones using (Eq. S1). Then, (x, y) value was calculated based on an international standard using (Eq. S2).

$$\begin{bmatrix} X \\ Y \\ Z \end{bmatrix} = \begin{bmatrix} 0.4124 & 0.3576 & 0.1805 \\ 0.2126 & 0.7152 & 0.0722 \\ 0.0193 & 0.1192 & 0.9505 \end{bmatrix} \begin{bmatrix} R \\ G \\ B \end{bmatrix} \quad \ldots \text{(Eq. S1)}$$

$$(x, y) = \left(\frac{X}{X+Y+Z}, \frac{Y}{X+Y+Z}\right) \ldots \text{(Eq. S2)}$$

The original value before applying any stresses was defined as x_0. An increment of x ($\Delta x = x - x_0$) was calculated for the color-changed samples.

Effect of the PEI concentration and molecular weight. The effects of the PEI concentration and molecular weight on the color-change behavior were studied with immersion of SR/PDA in the PEI solution for 0.5–29.5 h. The PEI concentration was changed to 5, 10, 20, 30, 40, and 50 wt% for $\bar{M}_w$ 3 × 10^2. The different molecular weight of branched PEI was purchased: $\bar{M}_w$ 6 × 10^2 (Nippon Shokubai, EPOMIN SP-006), $\bar{M}_w$ 1.8 × 10^3 (Nippon Shokubai, EPOMIN SP-018), and $\bar{M}_w$ 7.5 × 10^5 (Aldrich). After withdrawing the sample pieces, the photographs were taken to analyze the Δx value. Related to these reference experiments, HSP and its distance of PEI-water and PEI-PDMS were calculated using a commercial software (HSP-ip 5.0.03). The oligomers of PEI and PDMS were used for the calculation.

Application of compression stresses. P = 0.1 kPa–5 MPa were applied to DL/SR/PDA with the compressing rate 1.5 N s^{-1} using an automated tester (Shimadzu, EZ-LX). The stress was applied for 120 s. After releasing the stress, the remaining undeformed DL was removed using a handy air blower. The device was maintained for 24 h at room temperature. The further remining DL, *i.e.* the silica shell nanoparticles adsorbed on the surface of SR, was washed out by ethanol. The photograph of the top face was taken using iPhone 14. The color-changed center area of 8 × 8 mm was used for the image analysis with removing the 1 mm margins. The

relationship between P and Δx was prepared as the standard curve.

Stress-distribution imaging. Compression stresses were applied to the DL/SR/PDA device (30 × 30 × 3 mm) via plastic ornaments of lemon, orange, and grape attached on the probe of the tester with the specific force. The stresses were applied for 120 s. After 24 h, the remaining DL was removed by ethanol and then the photograph was taken. The top-face image 30 × 30 mm in size was divided into the frames 0.5 × 0.5 mm in size to estimate Δx on each frame. The Δx value was mapped in the L_x–L_y coordinate. As the reference, the cross section was prepared with cutting the color-changed SR/PDA device after removing DL.

UV-Vis spectrum of SR

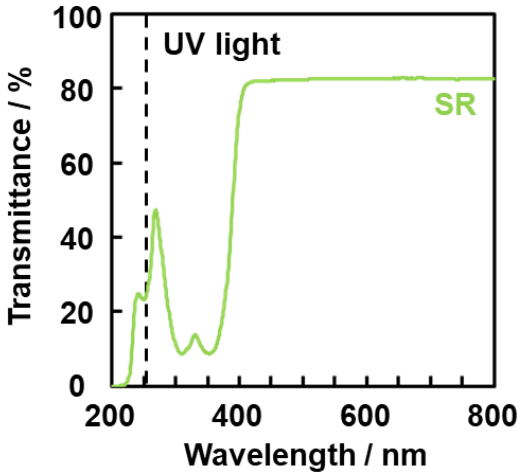

Fig. S2. UV-Vis spectrum of the SR matrix.

PCDA monomer crystals were dispersed in the SR matrix. The UV-Vis spectrum indicates that the SR matrix preserved the transparency in the UV region. The topochemical polymerization of PCDA was achieved with the UV-light irradiation at 254 nm.

Thermoresponsive color-change properties

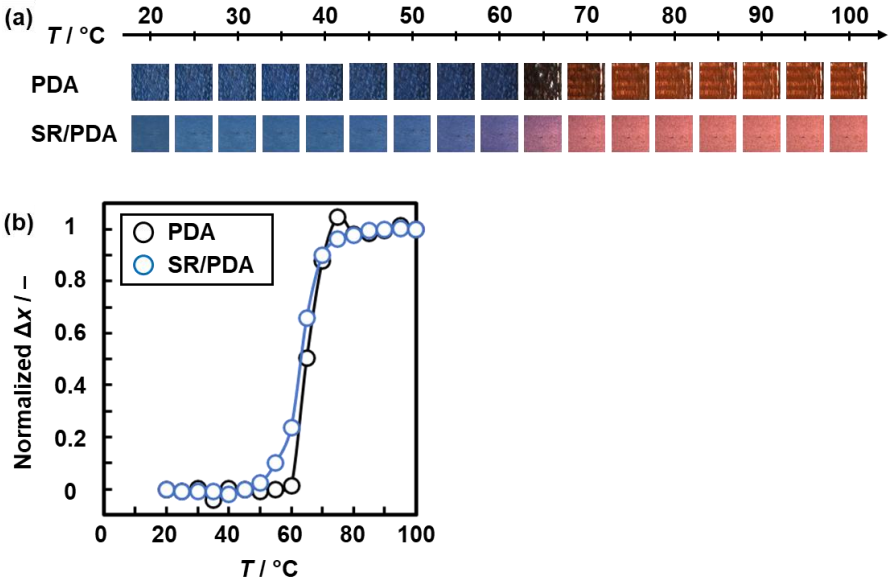

Fig. S3. Thermoresponsive color-change properties of PDA and SR/PDA. (a) Photographs. (b) Relationship between T and the normalized Δx.

The measured Δx was divided by the maximum value of Δx (Δx_{max}) to calculate the normalized Δx (Δx / Δx_{max}) in the vertical axis. Both PDA and SR/PDA showed the similar thermoresponsive color-transition properties at 65 °C.

Mechano-responsiveness of SR/PDA

Fig. S4. Photographs before (a) and after (b,c) compression of SR/PDA at 5 MPa.

No color change was observed for SR/PDA without combining DL even with applying the maximum $P = 5$ MPa in the calibration curve. The SR/PDA device was broken (Fig. S4a,b). An increment of red-color intensity (Δx) was calculated to 0.0086 on a piece of the fractured sample (Fig. S4c). The Δx value can be ignorable compared with that measured using the DL/SR/PDA device.

Color-change properties of SR/PDA immersed in PEI aq.

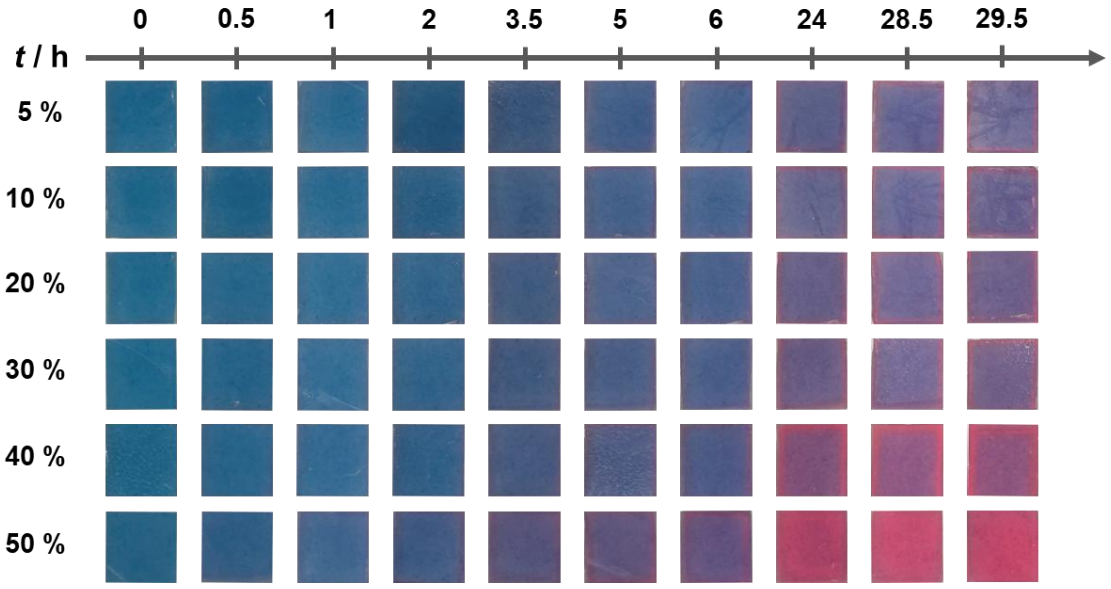

Fig. S5. Photographs of SR/PDA with the immersion in PEI ($\bar{M}_w$ 3 × 10^2) solution for 0.5–29.5 h at 5–50 %.

The color change to red was clearly visible for the naked eye at the PEI concentration 50 %. Based on the results, we set the PEI concentration at 50 % and time at 24 h for the color change.

SEM image of SR/PDA

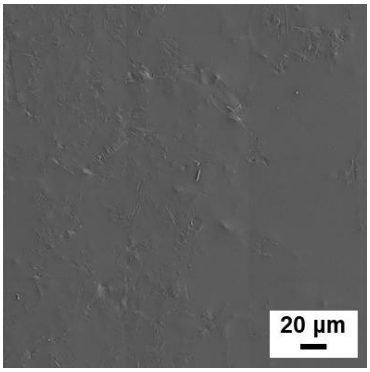

Fig. S6. Secondary electron (SE) image of SR/PDA.

The BSE image in the same area was displayed in Fig. 3d. Whereas the contrast differences originating from the composition, namely PDA and SR, were observed on the BSE image, the corresponding SE image showed the flat surface with the homogenous contrast. The SE image indicates that SR/PDA had no micrometer-scale cracks and voids to allow the rapid penetration of PEI.

Effect of PEI molecular weight on the color change properties

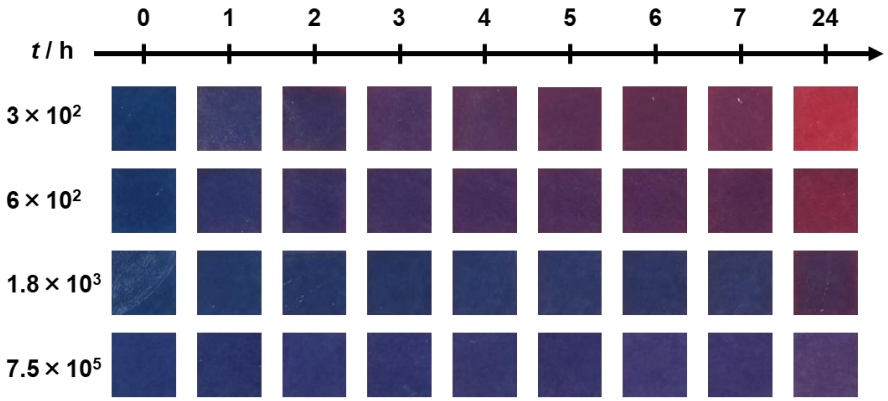

Fig. S7. Color-change properties of SR/PDA with the immersion for 1–24 h in the solution containing different molecular weight of PEI at 50 %.

The color-changing rate lowered with increasing the molecular weight of PEI. The fact implies that the diffusion of PEI through the free volume space in the SR matrix is delayed with an increase in the molecular weight.

PALS analysis of the SR matrix

Table S1. Summary of life time (τ_3), radius (r_3), and intensity (I_3).

	Life time τ_3 / ns	Radius r_3 / nm	Intensity I_3 / %
SR	3.46	0.393	37.0
PDA/SR	3.50	0.396	30.5

The free volume space was analyzed by the third contents (τ_3, r_3, I_3) of the PALS profile in Fig. 4f. PEI can be penetrated inside the SR matrix through the diffusion in the free volume space.

Deformation of the layered structure

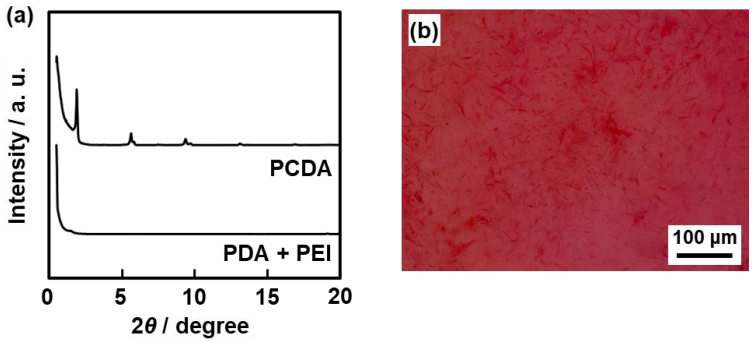

Fig. S8. Structural analyses of the layered PDA with the intercalation of PEI. (a) XRD patterns of the layered PCDA (upper) and PDA after the exposure to PEI solution. (b) Optical microscopy image of SR/PDA after the color change with the intercalation of PEI.

As a reference experiment, the PDA powder was exposed to the PEI solution. As the structural changes of the layered PDA were not clearly detected in the SR matrix, the reference experiment was performed using the powder of PDA. The XRD peaks characteristic of the layered structure disappeared with exposure to PEI (Fig. S8a). In addition, the size of PDA was 20.3 ± 8.0 μm after the color change (Fig. S8b). The significant size variation was not observed with the color change.

Color-change properties of SR/PDA with compression

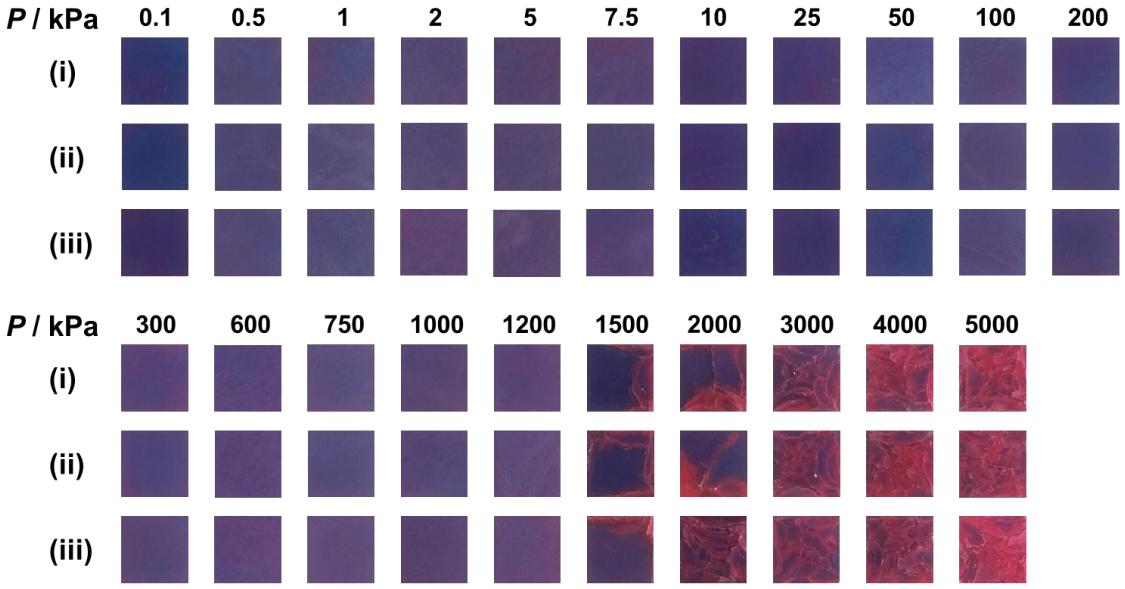

Fig. S9. Photographs of the SR/PDA samples with compression in the range of P = 0.1 kPa–5 MPa (N = 3).

Table S2. Relationship between P and Δx.

P / kPa	0.1	0.5	1	2.5	5	7.5	10	25	50	100	200
(i) Δx / –	0.0376	0.0298	0.0361	0.0333	0.0384	0.0436	0.0366	0.0481	0.0506	0.0515	0.0532
(ii) Δx / –	0.0275	0.0382	0.0341	0.0369	0.0382	0.0346	0.0444	0.0411	0.0486	0.0507	0.0567
(iii) Δx / –	0.0237	0.0330	0.0343	0.0406	0.0362	0.0402	0.0431	0.0415	0.0506	0.0496	0.0612
$\overline{\Delta x}$	0.0296	0.0337	0.0348	0.0369	0.0376	0.0395	0.0414	0.0436	0.0499	0.0506	0.0570
S. D.	0.0072	0.0042	0.0011	0.0037	0.0012	0.0045	0.0042	0.0040	0.0011	0.0010	0.0040
P / kPa	300	600	750	1000	1200	1500	2000	3000	4000	5000	
(i) Δx / –	0.0546	0.0611	0.0655	0.0644	0.0657	0.0836	0.1147	0.1175	0.1378	0.1334	
(ii) Δx / –	0.0594	0.0599	0.0626	0.0580	0.0656	0.0939	0.1087	0.1142	0.1332	0.1405	
(iii) Δx / –	0.0609	0.0613	0.0678	0.0684	0.0694	0.0816	0.1095	0.1125	0.1309	0.1384	
$\overline{\Delta x}$	0.0583	0.0608	0.0653	0.0636	0.0669	0.0864	0.1110	0.1147	0.1340	0.1374	
S. D.	0.0033	0.0007	0.0026	0.0052	0.0022	0.0066	0.0033	0.0025	0.0035	0.0037	

The Δx values in Fig. S9 were summarized in Table S2. The average values ($\overline{\Delta x}$) were used for preparation of the relationship between P vs. Δx in Fig. 5d.

Effect of the preservation time on the color-change properties

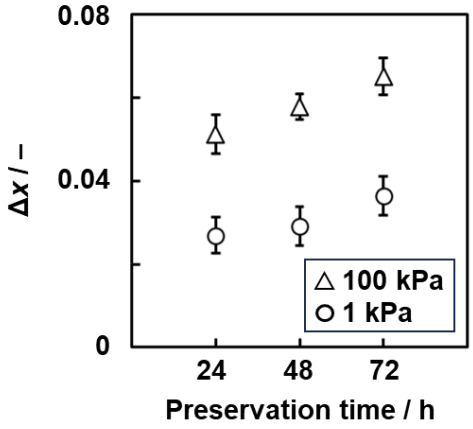

Fig. S10. Relationship between preservation time to taking the photographs and Δ*x*.

The SR/PDA device was immersed in the PEI solution to estimate an appropriate time to achieve the diffusion of PEI into SR (Fig. 4a). Based on the results, the preservation time to facilitate the diffusion was set to 24 h in the present work. When the preservation time was prolonged to 48 and 72 h (Fig. S10), an increase in Δ*x* was observed at *P* = 1 and 100 kPa. The diffusion of PEI into the SR matrix is continued even after 24 h. The color-changed samples are not stored. This DL/SR/PDA device needs to take the photographs at certain preservation time after the color change.

Estimation of the number of the disrupt DL

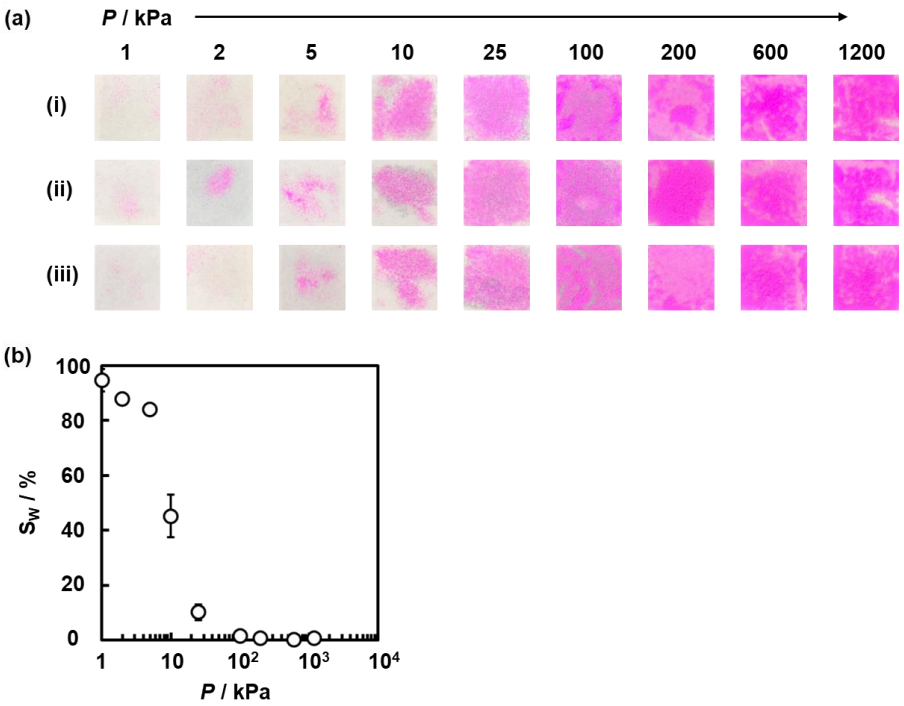

Fig. S11. Estimation of the number of disorganized DL. (a) Photographs (N = 3). (b) Relationship between P and white area (S_w / %).

Table S3. Relationship between P and S_w.

P / kPa	1	2	5	10	25	100	200	600	1200
(i) S_w / %	99.075	86.404	83.61	38.002	12.399	0.5255	0.9545	0.2623	0.0674
(ii) S_w / %	91.176	87.263	86.083	53.317	6.8837	1.2706	1.0845	0.3288	1.5349
(iii) S_w / %	93.651	89.551	82.097	44.146	10.939	2.6396	0.3411	0.1492	0.1998
$\overline{S_w}$ / %	94.634	87.739	83.93	45.155	10.074	1.4786	0.7934	0.2468	0.6007
S. D.	4.0401	1.6267	2.0122	7.7072	2.8577	1.0723	0.397	0.0908	0.8117

The colored DL was prepared with addition of rhodamine B in the interior liquid (10^{-3} mol dm^{-3}) in the same procedure as that of the non-colored DL. The colored DL (ca. 50 mg) was dispersed on 10 × 10 mm of a filter paper. The weight of DL and area of compression were same as those for DL/SR/PDA. After the compression, the photograph was taken without removal of the remaining DL. The percentage of the white-color area (S_w / %) was calculated from the images. The remaining white area corresponds to the amount of the remaining DL.

Quantitative correlation between *P* and each factor

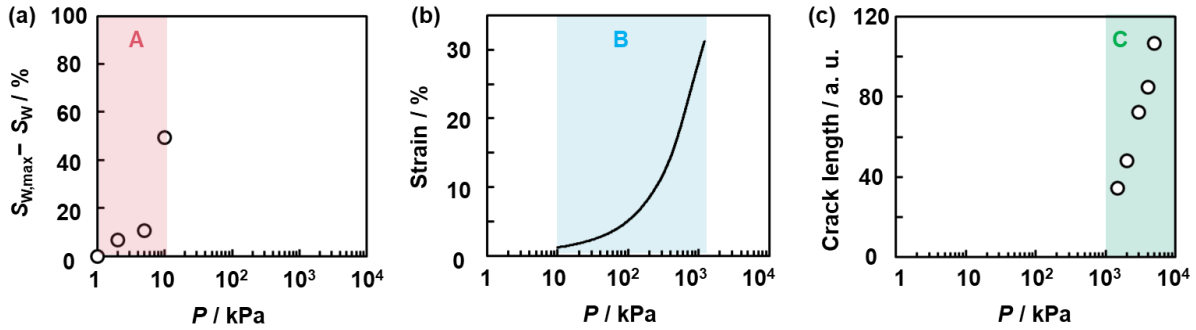

Fig. S12. Relationship between *P* and potential factors in the regions A–C. (a) Relationship between *P* and amount of the disrupt DL in the region A. (b) Relationship between *P* and strain in the region B. (c) Relationship between *P* and crack length in the region C.

In the region A, the amount of the remaining DL was estimated from the remaining white-color area (S_w) of the photographs (Fig. S11). The differences between S_w and maximum S_w ($S_{w,max}$) ($S_{w,max} - S_w$) indicate the amount of the disrupt DL. Fig. S12a shows the correlation between *P* and ($S_{w,max} - S_w$). As the strain is small in this region (Fig. 5d), the red-color intensity is mainly determined by the number of the disrupt DL, *i.e.* the amount of outflow PEI. In the region B, the strain significantly increased with increasing *P* (Fig. S12b). The penetration of PEI in SR is promoted in the strained state in the region B. In the region C, the cracks formed in SR as well as the strain increased (Fig. 5b–d). The generated cracks were visually recognized in the photographs. The amount of the cracks was estimated from the length (pixels) on the photograph with the same magnification. Fig. S12c shows the relationship between *P* and generated crack length. The correlation indicates that the amount of the cracks increased with increasing *P*. In this manner, the related factors have correlation with *P* in the regions A–C.

Cross-sectional images of the devices in the regions A and B

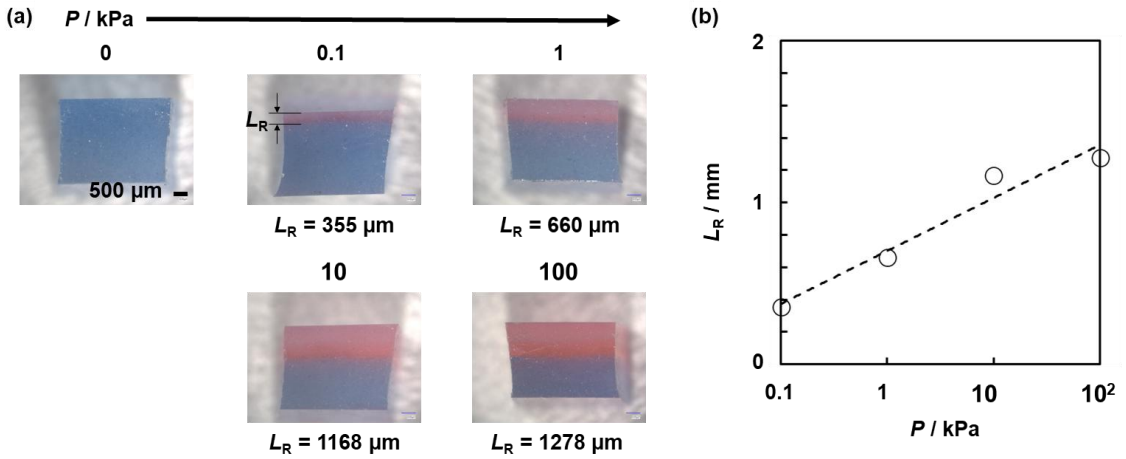

Fig. S13. Cross-sectional images of the devices after the applications of P = 0.1–100 kPa (a) and their relationship between P and depth of the red-colored area (L_R) (b).

The cross-sectional image shows that the red-colored area in the depth direction increased with increasing P (Fig. S13).

Standard curve for the boundary between the regions B and C

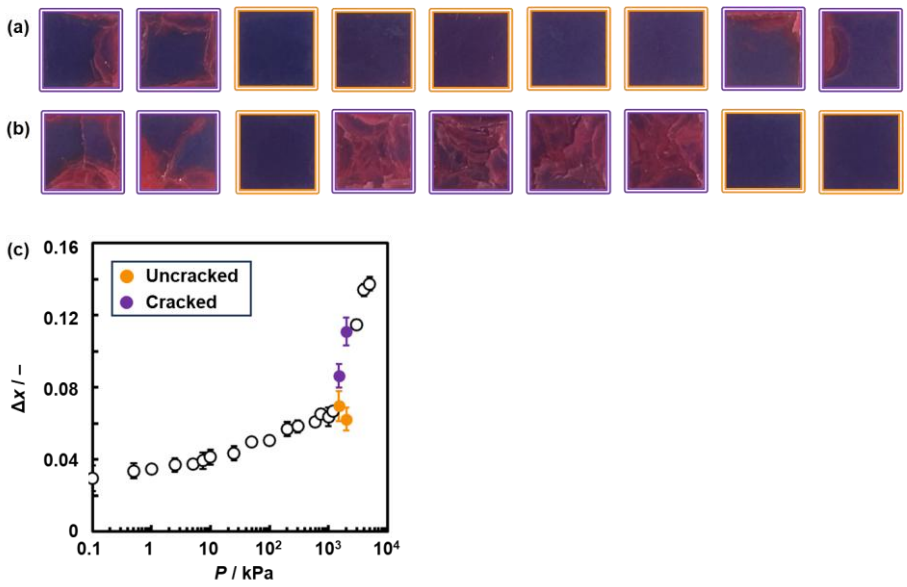

Fig. S14. Colorimetric estimation of P at the boundary between the regions B and C. (a,b) Photographs of the cracked (purple frame) and uncracked (yellow frame) SR/PDA devices after compressing 1.5 MPa (a) and 2.0 MPa (b). (c) Relationship between P and Δx with addition of the plots about the cracked and uncracked samples.

In the boundary between the regions B and C, the SR/PDA device sometimes generated the cracks (Fig. S14a,b). The preferred standard curves depend on whether the device has the cracks or not (Fig. S14c).

Colorimetric estimation of simulated unknown *P*

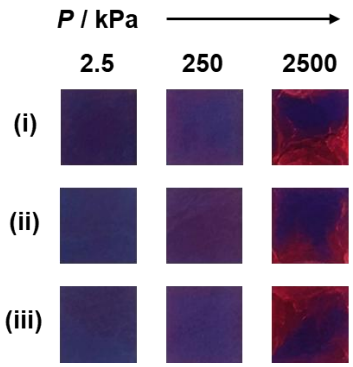

Fig. S15. Photographs of the SR/PDA device with the application of P = 2.5, 250, and 2500 kPa as simulated unknown stresses.

Table S4. Relationship between Δx and estimated P.

Ideal P / kPa	2.5	250	2500
(i) Δx / –	0.0349	0.0604	0.107
(ii) Δx / –	0.0331	0.0427	0.0775
(iii) Δx / –	0.0356	0.0546	0.112
$\overline{\Delta x}$	0.0345	0.0526	0.0987
S. D.	0.0013	0.0090	0.0186
Estimated P / kPa	0.992 ± 0.061	198 ± 213	1940 ± 767

The $\overline{\Delta x}$ and standard deviation (S. D.) were plotted with the colors in Fig. 5d.

Original data of compressing experiment

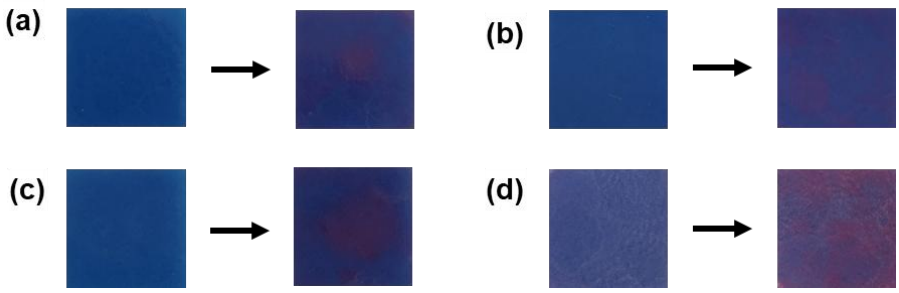

Fig. S16. Photographs of SR/PDA after compression using lemon (a,b), orange (c), and grape (d) after removal of DL. The left panels are the original photographs and right ones are the adjusted ones.

The image was adjusted to show the color-change behavior more clearly in the main text (Fig.6). In this adjustment, each *R*, *G*, and *B* value was equally increased with adding the same increment. This adjustment corresponds to controlling brightness of the image. The calculation of the x and Δx values for the quantification was carried out using the original images without the correction.

Cross sectional images of SR/PDA

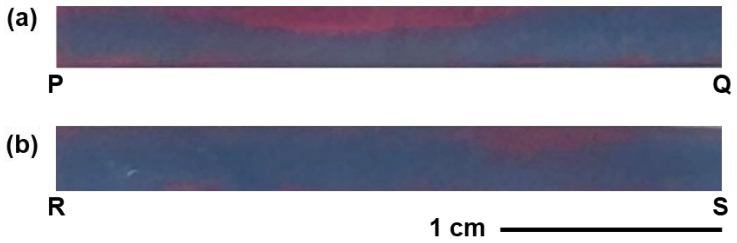

Fig. S17. Two cross-sectional images of the SR/PDA devices with cutting in the lines P-Q (a) and R-S (b) in Fig. 6h. The compression was performed using lemon near the center and corner, as shown in Fig. 6d,e, respectively.

The reference line profiles, L_x vs. Δx, were prepared using these cross-sectional images (red plots in Fig. 6h). The profiles in the same line were prepared from the 2D distribution using the top face images (blue plots in Fig. 6h). As the two profiles prepared by the different methods are consistent with each other, the stress distribution can be imaged using the surface image.